Five groups of esterase spots were recorded, according to electrophoretic migration:

(1) β_2-γ region: A slow esterase is present in some sera of pigeons and ducks[7]; it is inhibited by prostigmin M 10^{-5} for duck sera but not inhibited even by M 10^{-4} for pigeons. A somewhat faster esterase is present in all examined sera of guinea-fowl; it is inhibited by prostigmin.

(2) β_1 region (around the reservoir): Present in all sera; variable in intensity; more important in Gallinaceae than in other species; the most intense for pheasants and guinea-fowl sera; inhibited by prostigmin; the only spot coloured by butyrylthiocholine.

(3) α_2–α_1 region: Present in all sera; variable in intensity and mobility; the most important in Anatidae and pigeons; in these species no individual variations were observed; for turkeys, pheasants and hens (with exception of the M44 strain) small variations in intensity; in guinea-fowl sera there are two spots variable in intensity; in quail's sera, significant variations in number, intensity and mobility were encountered: some sera contain a slow α-esterase, some a fast α-esterase, some both of them and others none. All α-esterases are inhibited by the DFP and they are resistant to prostigmin.

(4) Albumin region: Some quail sera contain an esterase covering partially the albumin area.

(5) ϱ (rapid): This esterase, faster than albumin, is less frequent and less intense than the preceding one; not observed in hen, turkey or guinea-fowl sera, quite important in pheasants, it is also present in ducks and pigeons.

Although for some species there are individual variations, on the whole significant differences between species were observed. In some cases these were more striking than differences between proteinograms. Thus the esterase pattern appears as a sensitive technique for differentiation of bird species.

The intra-species variations observed might, on the other hand, be ascribed to the genetically determined families of components, as for example, transferrins, haptoglobins etc. An investigation is in progress on quail.

In some species quite uniform patterns were found which could be interpreted in terms of biological homogeneity of the strain examined, as for instance the M44. In the case of duck sera, however, the remarkable constancy of results was obtained with a considerable number of samples from animals of various races, and, as such, certainly not closely related. As their protein patterns were previously found variable[6,8], this discrepancy between esterases and main proteins would indicate that they do not correspond to the same phase of phylogenetic evolution[9].

Résumé. Les taches colorées correspondant à l'activité estérasique des sérums d'oiseaux, après électrophorèse en gélose, diffèrent entre elles en nombre, localization et relative intensité de coloration dans les sérums provenant de familles différentes: Poules, Canards, Pigeons ou d'espèces d'une même famille. Chez certaines espèces, on peut également observer des variations individuelles.

MARIE KAMINSKI
with the technical assistance of M. JEANNE-ROSE

Laboratoire de Histophysiologie du Collège de France, Paris (France), November 15, 1963.

1 J. PAUL and P. F. FOTTRELL, Ann. N.Y. Acad. Sci. *94*, 668 (1961).
2 J. URIEL, Ann. Inst. Pasteur *101*, 104 (1961).
3 N. TALAL, G. HERMANN, C. DE VAUX ST. CYR, and P. GRABAR, J. Immunol. *90*, 246 (1963).
4 G. HERMANN, N. TALAL, C. DE VAUX ST. CYR, and J. ESCRIBANO, J. Immunol. *90*, 257 (1963).
5 M. KAMINSKI and H. BALBIERZ, in preparation.
6 M. KAMINSKI and E. GAJOS, in *Proteins in Biological Fluids* (Elsevier, Amsterdam 1964), in press.
7 M. KAMINSKI, C. R. Acad. Sci. *257*, 2745 (1963).
8 M. KAMINSKI, Bull. Soc. Chim. Biol. *1964*, in press.
9 All Gallinaceae and ducks studied came from the Laboratoire de Photobiologie du C.N.R.S., Gif-sur-Yvette. Thanks are due to the whole staff for help in collecting blood samples.

The CO_2-Binding Capacity of Rat Brain Tissue *in vivo*

There has been no systematic determination of the CO_2-binding capacity of brain tissue *in vivo* and the scattered values which exist have been based on tissue material subjected to *post mortem* changes. It has been shown that accurate analysis of the acid-base metabolism of the brain requires that the tissue is frozen *in situ*[1,2]. Carbon dioxide dissociation curves on brain tissue homogenates, on the other hand, do not truly reflect the *in vivo* buffer capacity of the tissue, since this capacity may involve active transport mechanisms as well as metabolically induced changes of the tissue buffer systems. The present study, which is part of a systematic investigation of the acid-base metabolism of brain tissue, describes the CO_2-binding capacity of rat brain tissue exposed to arterial carbon dioxide tensions of 12–107 mm Hg.

Methods. The experiments were performed on rats of the Sprague-Dawley strain which were anaesthetized with Nembutal (40–50 mg/kg body weight) and tracheotomized. The rats were exposed to various carbon dioxide concentrations for 5–180 min. Low arterial carbon dioxide tensions were induced in some animals by artificial hyperventilation with a Palmer Miniature Ideal Respiration Pump. The other rats were allowed to breathe spontaneously and they were given gas mixtures containing 0–12% carbon dioxide in an open system. The acid-base parameters in arterial blood were measured in samples drawn from a cannula in the femoral artery, using the micromethod of SIGGARD ANDERSEN et al.[3]. Blood analyses were performed before and at repeated intervals during the exposure of the animals to the altered P_{CO_2}. At the end of the experiment the head of the animal was dipped into liquid nitrogen. The total carbon dioxide content of the brain was determined with the method recently

1 U. PONTÉN and B. K. SIESJÖ, Exper. *19*, 312 (1963).
2 U. PONTÉN and B. K. SIESJÖ, Acta physiol. scand., in press.
3 O. SIGGARD ANDERSEN, K. ENGEL, K. JÖRGENSEN, and P. ASTRUP, Scand. J. clin. lab. Invest. *12*, 172 (1960).

published from this laboratory[4]. The carbon dioxide tension of the brain tissue (P_{tCO_2}) was estimated from the arterial P_{CO_2} by assuming the mean tissue carbon dioxide tension to be 1 mm Hg above the mean capillary carbon dioxide tension[5]. The calculation of the mean capillary P_{CO_2} is described elsewhere[6]. The values for the total carbon dioxide content of the brain tissue were corrected for a blood content of 3%[7]. No other corrections were made for reasons discussed elsewhere[8]. The solubility factors used were 0.0301 μmoles/g/mm Hg for arterial blood, 0.0292 for brain tissue and 0.03135 for the water phase of the brain tissue[9].

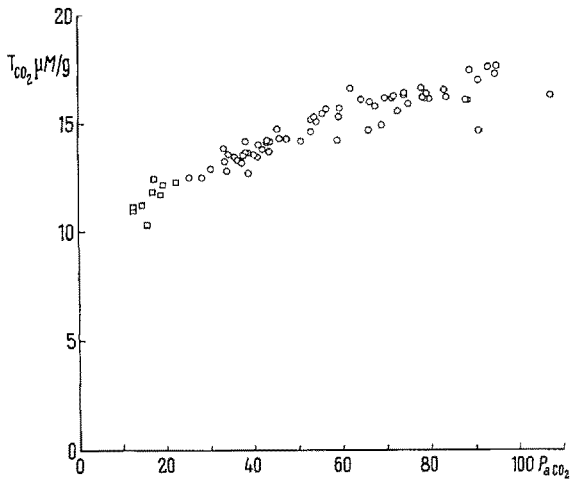

Fig. 1. Relation between the arterial carbon dioxide tension and the total carbon dioxide content in rat brain tissue. The animals were either artificially hyperventilated (squares) or were breathing spontaneously (circles). The latter were given 0–12% CO_2 in an open system.

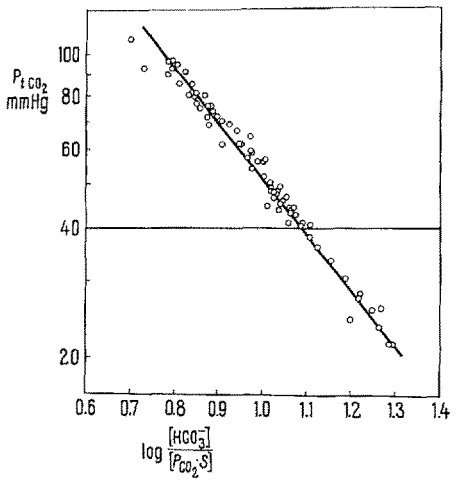

Fig. 2. Relation between the tissue carbon dioxide tension (logarithmic coordinates) and the logarithm of the buffer ratio $[HCO_3^-]/[P_{tCO_2} \cdot S]$ (see text). The slope of the line

$$\log \frac{[HCO_3^-]}{[P_{tCO_2} \cdot S]} = 2.36 - 0.79 \log P_{tCO_2}$$

denotes the buffer capacity for carbon dioxide.

Results. The P_{CO_2} of the arterial blood reached a steady level in less than 30 min of exposure to the altered alveolar carbon dioxide tension. The 73 rats used for the construction of the carbon dioxide dissociation curve were exposed to the various carbon dioxide tensions for 30–180 min.

Figure 1 gives the 'dissociation curve' in its conventional form where the parameters actually measured have been plotted, i.e. the arterial P_{CO_2} and the total carbon dioxide content of the brain tissue.

Figure 2 gives the relation between the mean tissue carbon dioxide tension (P_{tCO_2} mm Hg) in logarithmic coordinates and the logarithm of the buffer ratio $[HCO_3^-]/[P_{tCO_2} \cdot S]$ where $[HCO_3^-]$ and $[P_{tCO_2} \cdot S]$ are the mean bicarbonate and the mean carbonic acid concentration in μmoles/g of water in the tissue, respectively. Statistical calculations assuming a linear regression gave a coefficient of correlation of −0.989 and the regression equation

$$\log \frac{[HCO_3^-]}{[P_{tCO_2} \cdot S]} = 2.36 - 0.79 \log P_{tCO_2}$$

A P_{tCO_2} value of 40 mm Hg corresponds to a bicarbonate concentration of 15.5 μmoles/g of water in the tissue.

Discussion. The slope of the line in Figure 2 denotes the buffer capacity of the supratentorial parts of the rat brain tissue, including any extracellular fluid and also the amount of cerebrospinal fluid present. Since the knowledge of the size and the composition of the extracellular space is still very incomplete and since the cerebrospinal fluid does not behave as a simple salt solution in the buffering against carbon dioxide[10,11], no correction has been applied for these compartments. The buffer capacity of the brain tissue is much lower than that of whole blood and even a little less than that given for cortical tissue homogenates[12]. The latter might be explained by different amounts of cerebrospinal fluid in the analysed materials.

The regression in Figure 2 is treated as a linear one which is an approximation without practical significance in the P_{CO_2} range used here.

Knowledge of the buffer capacity of brain tissue for carbon dioxide makes it possible to differentiate between respiratory and non-respiratory acid-base changes in the tissue. Thus, respiratory changes are adequately described by the P_{CO_2}, while non-respiratory changes are defined by parallel displacements of the buffer line. These changes can then easily be expressed as changes in the bicarbonate concentration at a defined P_{CO_2}, i.e. as changes in the standard bicarbonate[8,13].

[4] U. PONTÉN and B. K. SIESJÖ, Acta physiol. scand., in press.
[5] U. GLEICHMANN, D. H. INGVAR, D. W. LÜBBERS, B. K. SIESJÖ, and G. THEWS, Acta physiol. scand. *55*, 127 (1962).
[6] U. PONTÉN, to be published (1964).
[7] N. B. EVERETT, B. SIMMONS, and E. P. LASHER, Circulation Res. *4*, 419 (1956).
[8] B. K. SIESJÖ and U. PONTÉN, to be published (1964).
[9] B. K. SIESJÖ, Acta physiol. scand. *55*, 325 (1962).
[10] C. R. MERWARTH and H. O. SIEKER, J. appl. Physiol. *16*, 1016 (1961).
[11] A. G. SWANSON and H. ROSENGREN, J. appl. Physiol. *17*, 812 (1962).
[12] B. K. SIESJÖ, Acta neurol. scand. *33*, 98 (1962).
[13] *Acknowledgments.* This investigation was supported by grants from the Medical Faculty of Lund and by the Swedish Medical Research Council and by Contract N 62558-3954 between the Office of Naval Research, Department of the U.S. Navy, and the University of Lund.

Zusammenfassung. 73 Ratten wurden hyperventiliert und mit Gasgemischen verschiedener CO_2-Gehalte (0–12%) während 30–180 min beatmet (arterieller P_{CO_2} 12–107 Torr). Die Versuchstiere wurden *in situ* eingefroren und der CO_2-Gehalt des Gehirngewebes mit eigener Methode bestimmt. Dissoziationskurve und Pufferkapazität des Gehirngewebes für CO_2 *in vivo* werden mitgeteilt.

U. PONTÉN

Departments of Neurological Surgery, University of Lund (Sweden), January 23, 1964.

Pronephric System in Haploid and Diploid Larvae of *Xenopus laevis*

DALCQ[1] suggested that the oedema which develops in about 90% of haploid frog tadpoles is the result of blockage, and consequently malfunction, of the pronephric system. However, in our experience with *Xenopus laevis* such oedematous tadpoles have greatly swollen, but apparently patent pronephric tubules and Wolffian ducts, and it seemed possible that the oedema might be caused rather by increased water uptake than by reduced elimination. If this were so, the occasional haploid embryo developing without oedema might owe its health to an exceptionally active nephric system. If the haploid kidney is having to eliminate more water than a diploid in order to prevent the development of oedema, it might become hypertrophied in the way that the remaining kidney does after unilateral pronephrectomy in diploid *Triturus* (FOX[2]). We therefore compared the structure of the pronephric systems of five haploid tadpoles showing fairly normal development and no oedema with those of five control diploids. The measurements were made on longitudinal and transverse serial sections, and are summarized in the Table. All the differences between the haploids and diploids there shown are significant.

We agree with FANKHAUSER[3] who suggested, as a result of his studies on haploid salamanders, that there is a tendency for haploid organs to compensate for small cell size by an increase in cell number. However, it was found that the haploid pronephric system in *Xenopus* not only compensated, but over-compensated. Our figures show a 16% superiority in total cell volume in haploids and a corresponding increase of 140% in cell numbers. Comparable figures for hypertrophied and hyperfunctional *Triturus* diploid pronephros[2] were 34% and 17%.

Thus we feel justified in suggesting that, since the pronephric system of non-oedematous haploid tadpoles is hypertrophied and possibly hyperfunctional, the oedema so often seen in haploids may not, in fact, be caused by kidney dysfunction, but rather by failure to cope with a quite exceptional functional demand.

Zusammenfassung. Eine morphologische Untersuchung des Vornierensystems in haploiden und diploiden Xenopuslarven weist darauf hin, dass das haploide Oedem nicht durch eine Funktionsstörung des Vornierensystems verursacht ist.

H. FOX and LOUIE HAMILTON

Department of Zoology, University College, London, and Department of Biology, Middlesex Hospital Medical School, London (England), January 10, 1964.

[1] A. DALCQ, Arch. Biol. Liège et Paris *43*, 343 (1932).
[2] H. FOX, J. Embryol. exp. Morph. *4*, 139 (1956).
[3] G. FANKHAUSER, Quart Rev. Biol. *20*, 20 (1945).

Measurements and calculations of various components of the pronephric system of diploid and haploid larvae of *Xenopus laevis* (five animals in each group)

	Pronephros		Pronephric duct	
	diploid	haploid	diploid	haploid
Mean antero-posterior length (mm)	0.243 ± 0.0099	0.279 ± 0.0124	0.562 ± 0.0160	0.436 ± 0.0310
Mean nuclear population	1337 ± 57	3159 ± 257	276 ± 7	793 ± 43
Mean total volume of cells ($mm^3 \times 10^{-3}$)	3.2 ± 0.21	3.7 ± 0.33	0.37 ± 0.020	0.60 ± 0.044
Mean total volume of lumina ($mm^3 \times 10^{-3}$)	1.5 ± 0.11	2.5 ± 0.14	0.21 ± 0.011	0.49 ± 0.062
Mean internal surface area of lumina (mm^2)	0.2236 ± 0.01521	0.2450 ± 0.01679	0.0415 ± 0.00117	0.0604 ± 0.00522
Mean volume of individual cell (μ^3)	2419 ± 128	1194 ± 79	1353 ± 76	761 ± 49
Mean anterior-posterior nuclear length from horizontal section (500 pronephros, 200 duct) (μ)	8.87 ± 0.051	6.59 ± 0.047	8.59 ± 0.078	6.35 ± 0.070
Mean nuclear diameter from transverse section (800) (μ)	6.56 ± 0.021	5.18 ± 0.017	6.54 ± 0.023	5.18 ± 0.017
Calculated nuclear volume (μ^3)	300	139	290	134
Calculated nucleo-cytoplasmic volume ratio	0.142	0.132	0.273	0.214
Calculated nuclear surface area (μ^2)	250	149	243	145
Calculated volume (μ^3) of cytoplasm/1 μ^2 nuclear surface	8.5	7.1	4.4	4.3
Calculated length/breadth nuclear index	1.352	1.272	1.313	1.226